ECS Transactions, 57 (1) 1781-1791 (2013)
10.1149/05701.1781ecst ©The Electrochemical Society

Electronic Activation At Oxide Hetero-structure At Elevated Temperatures – Source Of Markedly Accelerated Oxygen Reduction Kinetics

Y. Chen[a], Z. Cai[a], Y. Kuru[a,b], H. L. Tuller[b] and Bilge Yildiz[a]

[a]Laboratory for Electrochemical Interfaces, Department of Nuclear Science and Engineering, Massachusetts Institute of Technology
[b]Department of Materials Science and Engineering, Massachusetts Institute of Technology 77 Massachusetts Avenue, Cambridge, MA 02139, USA

To understand ultra-fast oxygen reduction reaction kinetics near $La_{0.8}Sr_{0.2}CoO_3/(La_{0.5}Sr_{0.5})_2CoO_4$ ($LSC_{113/214}$) interface, a combination of *in-situ* scanning tunneling spectroscopy and focused ion beam milling was used to study the local electronic structure near $LSC_{113/214}$ interface at elevated temperature and in oxygen. The electronic activation of LSC_{214} by the coupling with LSC_{113}, concurrent with the fast oxygen incorporation on LSC_{214}, was identified to be a key reason. These results put forward the electronically coupled oxide structures as novel cathodes. We generalize and further test this idea on a $La_{0.8}Sr_{0.2}CoO_3/La_2NiO_4$ system, which shows a similar electronic activation of La_2NiO_4 at elevated temperatures.

Introduction

Solid Oxide Fuel Cells (SOFCs) are particularly attractive for a sustainable energy infrastructure because of their fuel flexibility and high conversion efficiency (1). The high working temperature of SOFCs (800-1000°C), on one hand, makes this kind of fuel cell very efficient because of faster transport and electrochemical reaction kinetics. On the other hand, such high temperatures create problems because of the aging and durability of issues of materials. In order to decrease the cost for the SOFCs, it is desirable to decrease the working temperature of SOFCs to intermediate range (500-750 ^oC). At such low temperatures, the oxygen reduction reactions (ORR) at cathodes are reported to be the main barrier for SOFCs to achieve high performance. Therefore, it is needed to synthesize cathode materials with high oxygen reduction activity at reduced temperatures (<700 ^oC). Traditional approaches to enhancing cathode performance include the tailoring of crystal structure, chemical composition, and microstructure, such as the use of porous nanostructured composites (2). Recent reports of oxide hetero-structures exhibiting exceptionally high ORR activity and ionic conductivity give a promising alternative approach to achieve high-performance cathodes. An example is the $(La,Sr)CoO_3/(La,Sr)_2CoO_4$ ($LSC_{113/214}$) hetero-structure. Spatially resolved Secondary Ion Mass Spectrometry (SIMS) (3,4) and electrochemical measurements (5,6) have demonstrated oxygen exchange kinetics several orders of magnitude faster near the interfaces between LSC_{113} and LSC_{214} thin layers at about 500 °C compared to either material individually. It is evident that the interfacial regions of these $LSC_{214/113}$ hetero-structures are responsible for such impressively accelerated ORR kinetics (7,8). This

paper summarizes our recent findings from experiments (9) and computation (7) to uncover the physical origin of these empirically observed results.

The objective of this work is to obtain a fundamental and micro scale understanding of the role of interfaces in determining the ORR activity of $LSC_{113/213}$ hetero oxide. We particularly focus on studying the correlation between the local electronic structure near the $LSC_{214/113}$ interface and the charge transfer process during ORR. Consequently, based on such understanding, we aim to design novel oxide hetero-structure as highly active cathode materials for the development of more efficient and durable SOFCs.

The key step of this research is to identify the local electronic structure near the $LSC_{113/214}$ interface at conditions close to that of the functional environment of SOFCs. Such information has been reported in previous studies to be a key feature governing the ORR activity (9-12). However, probing the electronic structure near an interface confined at the nanometer scale is a well-known challenge in the study of hetero-interfaces. To perform such experiments *in situ* at high temperature and in an oxygen environment has been beyond the traditional regime of materials characterization techniques. Scanning probe techniques are ideal in revealing local electronic, magnetic or electrochemical properties on the surface (13-15). However, it is very challenging to apply them to probe interfaces buried beneath the surface and under the harsh working conditions of SOFCs cathodes (high temperatures and in oxygen environments). Previous successful attempts at exposing the local interface properties of oxides to scanning probe characterization have not provided a generalized capability to expose buried interfaces in a controllable fashion and have been limited to room temperature measurements (14,15).

In this work, we combine *in situ* scanning tunneling microscopy and spectroscopy (STM/STS) with grazing incidence focused ion beam (FIB), for the first time, to overcome the challenges in accessing the local electronic structure of multilayer (ML) interfaces with high spatial resolution at elevated temperatures in oxygen gas environment (9,16). We found that at 200-300 ^{o}C, the LSC_{214} layers are electronically activated through interface coupling with LSC_{113}. Such electronic activation is expected to facilitate charge transfer to oxygen, and concurrent with anisotropically fast oxygen incorporation on LSC_{214}, explains the vastly accelerated ORR kinetics near the $LSC_{113/214}$ interface. Similar electronic activation behavior of La_2NiO_4 was also found in $La_{0.8}Sr_{0.2}CoO_3/La_2NiO_4$ system, with implications for enhanced ORR kinetics.

Experiment

The approach we used to probe the electronic structure near the hetero-interface at high temperature and in oxygen gas environment is schematically shown in Fig. 1 (16). Firstly, we fabricated a multilayer (ML) by pulsed laser deposition (PLD) to serve as a model system. The grazing incidence focused ion beam (FIB) milling was then used to expose buried interfaces to the surface, as shown in Fig. 1 (b). After FIB milling, 1keV Ar^+ sputtering following by annealing in oxygen was used remove any residual Ga^+ on the surface during FIB milling process. Fig. 1 (b) and (c) shows the side view and top view of the FIB cut region. We can see from Fig. 1 that hetero-interface region was expanded from nm to μm, which greatly facilitated the characterization of electronic structure near the interface by STM at elevated temperature. By applying either a positive

or a negative bias voltage to the STM tip, the filled and empty electronic states are detected. Consequently, we can identify the electronic density of states across the interface that has been exposed by FIB milling. This information correlates to the ease of electron transfer between surface and oxygen in ORR. Unique to our study is that we performed the STM/S measurements using a customized surface science system at elevated temperature and in an oxygen environment, which is relevant to the SOFC working conditions.

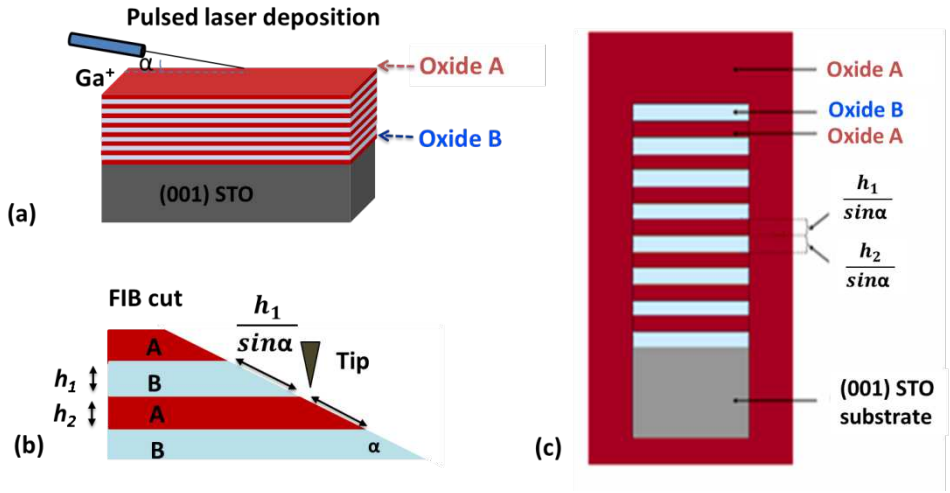

Figure 1. a) Schematic description of the FIB milling process with a shallow incidence angle, α, which was used to expose and visualize the inner layers and the interfaces. b) The side view of the multilayer specimen after FIB milling c) The top view of the multilayer after the FIB milling. The area of each layer, h_1 and h_2, is magnified by a factor of 1/sinα after FIB milling. Figure adapted from ref. (16)

The PLD was performed using a KrF excimer laser with wavelength of 248 nm. The films were deposited at 700 ^{o}C under 10 mTorr oxygen pressure. After the growth process, the films were cooled down to room temperature in 2 Torr oxygen pressure to oxidize the films. The FIB milling was carried out using the Helios Nanolab 600 dual beam FIB milling system. The Ga^{+} beam current and acceleration were 100 pA and 30 kV, respectively. The angle between the beam and surface were carefully aligned to be less than 1^{o}. A Physical Electronics Model 700 scanning nano-probe Auger Electron Spectrometer (AES) was used to spatially quantify the cation chemistry and the Ga content on the FIB-milled ML cross-section. The energy and current of incident electrons were 10 keV and 10 nA, respectively. No residual Ga was found in the FIB-cut region after Ar sputtering.

For identifying the crystal structure, the 2ϴ-ω scans were measured by a high resolution four circle Bruker D8 Discover diffractometer, equipped with a Göbel mirror, 4-bounce Ge (022) channel-cut monochromator, Eulerian cradle, and a scintillation counter, using Cu $K\alpha_1$ radiation.

A modified variable-temperature scanning tunneling microscope (VT-STM) (Omicron GmbH, Germany) was used to probe the surface morphology and to obtain surface electronic structure information with high spatial resolution at elevated temperatures (room temperature to 300 ^{o}C) and in oxygen environment (10^{-3} mbar). A retractable oxygen doser placed near the STM stage in the chamber was used to directly expose the

sample to oxygen during the STM/STS measurements. For surface cleaning and in-situ measurements, samples were heated using a pyrolytic boron nitride (PBN) heater. To obtain high quality images and tunneling spectra, the sample was cleaned prior to the STM/STS experiments by first sputtering the surface by low energy Ar^+ (0.5 keV) for 5 minutes, followed by heating in high purity oxygen at 450 ^oC and 10^{-3} mbar pressure for 1 hour. This served to remove the water and carbon-related adsorbates from the surface due to air-exposure after film growth.

An Omicron EA 125 hemispherical analyzer and Omicron DAR 400 Mg/Al dual anode non-monochromated X-ray source were used for the x-ray photoelectron spectroscopy (XPS) measurements probing the surface chemistry. An Mg K X-ray source (1253.6 eV), operated at 300 W, was used for all the XPS data shown in this paper. Peak-fitting and chemical quantification were performed using the CasaXPS 2.3.15 software.

Results and Discussion

Structure and Composition of $LSC_{113/214}$ Multilayer Model System

10 nm $La_{0.2}Sr_{0.8}CoO_3$ (LSC_{113}) and 10 nm $(La_{0.5}Sr_{0.5})_2CoO_4$ (LSC_{214}) multilayer (ML) with 10 modulations were grown on $SrTiO_3$ (STO) (001) by PLD. The LSC_{113} and LSC_{214} single phase were also grown on STO (001) substrate at the same condition to serve as reference samples, as shown in Fig. 2 (a). Both the LSC_{214} and LSC_{113} layers in the ML structure and in single phase were highly textured in the [001] out of plane direction. The 2θ-ω scan of $LSC_{113/214}$ multilayer is shown in Fig. 3.

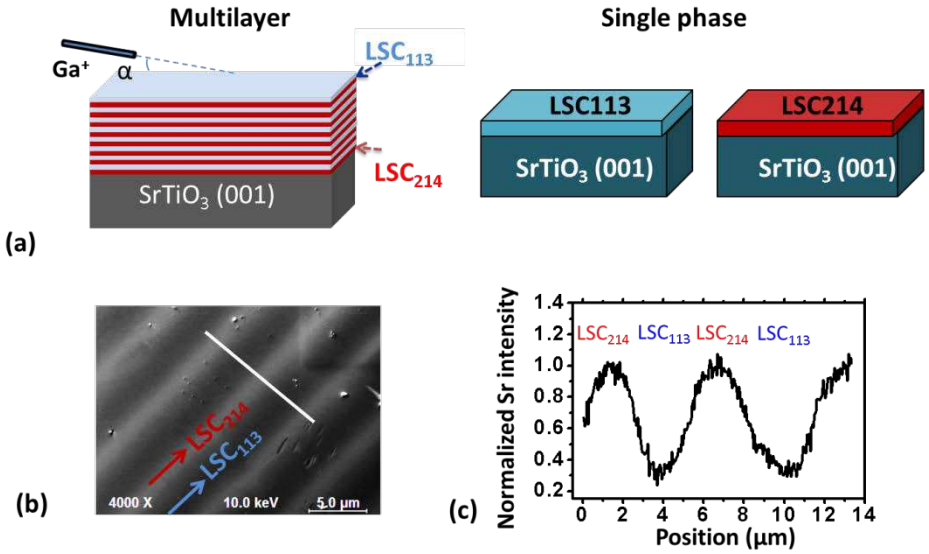

Figure 2. (a) Structure of $LSC_{113/214}$ multilayer and single phase reference samples (b) Scanning Electron Microscopy (SEM) image of the $LSC_{113/214}$ multilayer cross-section after FIB milling. (c) Sr intensity as function of position (tracing white line in (b)) measured by Auger electron spectroscopy (AES) line scan. The Sr intensity is normalized to that on the LSC_{214} phase in the multilayer structure. Figure adapted from ref (9).

The buried $LSC_{113/214}$ interfaces in ML structure are exposed to the surface by grazing incidence FIB milling to facilitate STM/STS characterization(16), as shown in Fig. 2 (a) and (b). Consistent differences in cation composition between the LSC_{214} and LSC_{113} layers are observed in the AES line scan across the interface (Fig.2 (c)). The surface cation composition of the LSC_{113} on the top surface layer and that on the exposed cross-section of the ML region are found to be the same, within the quantification error limits of the high-spatial-resolution AES. This indicates that the FIB milling process did not induce any detectable composition change within the layers.

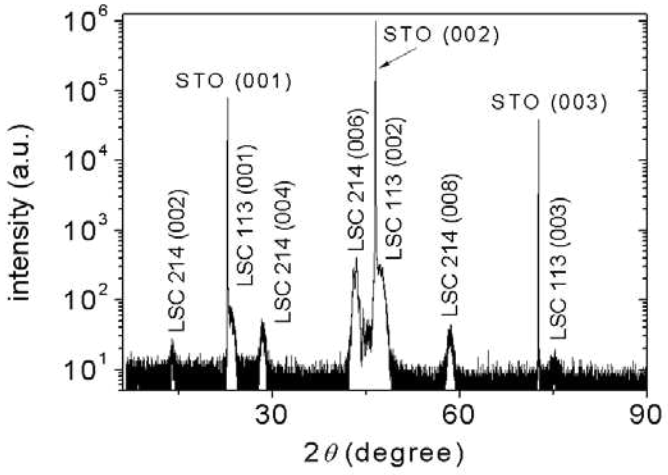

Figure 3. X-ray diffraction pattern of the $LSC_{113/214}$ ($La_{0.8}Sr_{0.2}CoO_3/(La_{0.5}Sr_{0.5})CoO_4$) multilayer sample between 10 and 80°, showing the 00*l* reflections of the LSC_{214} and LSC_{113} layers in the multilayer structure and of the STO substrate. The X-ray source is Cu Kα1 radiation. Figure adapted from ref. (9).

Electronic Structure near $LSC_{113/214}$ interface from Room Temperature to Elevated Temperatures

Fig. 4 (a) shows the topography measured by STM (top row) and the tunneling current map (bottom row) near an interface region of the $LSC_{113/214}$ ML system at room temperature and at 300 ^{o}C. At room temperature, we can see two distinct electronic regions from the tunneling current map between the LSC_{113} and LSC_{214} (Fig. 4(a), RT). Such contrast in the tunneling current maps correlates well with the spatial transitions in the STM topography images. This result indicates that there is a large difference in the electronic structure between LSC_{113} and LSC_{214} phase at room temperature. At 300 ^{o}C, the electronic structure contrast between the two phases was found to disappear, as shown in the (Fig. 4 (a)). Such change electronic structure can be seen more clearly from the band gap value measured from tunneling current spectra, as shown in Fig. 4 (b). The energy gap values are found to be 1.4 ± 0.2 eV on the LSC_{113} layers and 2.6 ± 0.3 eV on the LSC_{214} layers at room temperature. The energy gap of LSC_{113} in this ML structure is consistent with the energy gap value we previously reported as 1.5 ± 0.2 eV at room temperature on the surface of LSC_{113} single phase epitaxial thin films grown on STO (001) (17). As the temperature increases, the energy gaps of both LSC_{113} and LSC_{214} phases in ML structure decrease with increasing temperature and disappear at about 250 ^{o}C. When the samples are cooled down, the energy gap of both phases return to their

initial values (Fig. 4 (b)). Because of the reversibility of these transitions, this behavior can only be captured with *in situ* measurements.

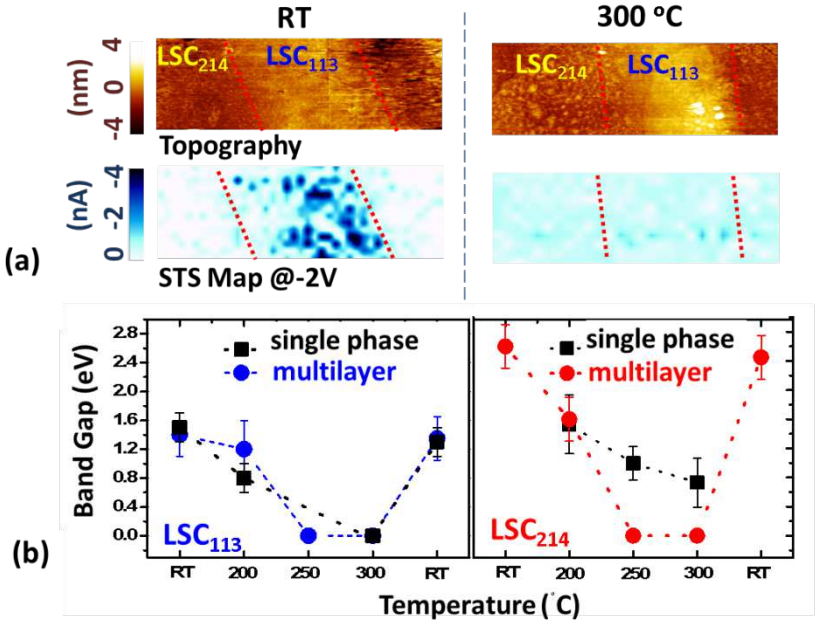

Figure 4. (a) Topography (top row) and tunneling current map (bottom row) at V_{tip}= -2 V from room temperature (RT) to 300 °C under oxygen pressure of 10^{-3} mbar. (b) Energy gap values obtained on LSC_{113} and LSC_{214} when they are within the ML structure versus values obtained for the single phase thin film structures. Figure adapted from ref. (9).

Fig. 4 (b) shows the comparison of band gap value for LSC_{113} and LSC_{214} in ML structure and in single phase. We can see that the LSC_{113} surface electronic structure in the ML structure behaves very similarly to its single-phase counterpart at high temperatures (17), while the electronic structure of LSC_{214} in the ML differs significantly by showing a reversible disappearance of the energy gap at and above 250 °C (Fig. 4 (b)).[1] The energy gap of the LSC_{214} phase at 200 °C in the ML structure decreases to 1.6 ± 0.2 eV, close to the energy gap of the LSC_{214} single phase thin film at the same temperature. Further increase of temperature to 250°C leads to the disappearance of the energy gap of the LSC_{214} in the ML structure. In contrast, the single phase LSC_{214} thin film still exhibits an apparent energy gap of 1.0 ± 0.2 eV at 250 °C and 0.8 ± 0.3 eV at 300 °C. This indicates that the presence of LSC_{113} influences the LSC_{214} electronic structure and activates it electronically through a coupling at their interface.

Mechanism of Electronic Activation in $LSC_{113/214}$ system

The disappearance of band gap on LSC_{113} single phase at high temperature has been previously reported by our group to be related to the reduction-induced oxygen vacancy defect states on LSC_{113} surface (17). Similar phenomenon was also reported for $La_{0.7}Sr_{0.3}MnO_3$ (18) and $Sr(Ti,Fe)O_3$ (19) thin films in our recent work. Because the LSC_{113} surface energy gap changes in a similar way with temperature in the ML and

[1] As mentioned above, the LSC_{214} single phase thin film was too insulating for STM/STS measurements at room temperature, thus, an energy gap value it is not reported specifically at RT before and after the high-temperature experiments.

single phase thin films, its decrease and disappearance in the ML is also likely due to the creation of oxygen vacancies in its near surface region.

LSC_{214} accommodates interstitial oxygen defects rather than oxygen vacancies for Sr content ≤ 50 % on the A-site (7,20). The reduction enthalpy in the LSC_{214} is considered to be higher than that in LSC_{113} (7). To confirm this, we compared the valence states of the Co cation which are directly correlated with the oxygen vacancy content in these two phases. A significant reduction of Co on the LSC_{113} film surface is evident from the appearance of the Co^{2+} satellite peak at about 300 ^{o}C (Fig. 5). On the contrary, the Co 2p spectrum on the LSC_{214} (Fig. 5) does not change between 200 to 300 ^{o}C. These results demonstrate that the formation of oxygen vacancies and the reduction of Co in the LSC_{214} phase are more difficult than that in the LSC_{113} phase, consistent with the theoretical results of our group (7). Therefore, the disappearance of the energy gap on the LSC_{214} layers in the ML structure cannot occur due to a significant reduction of Co on LSC_{214} at 200-300 ^{o}C.

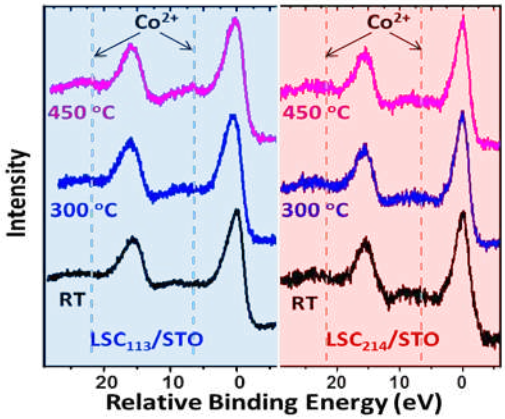

Figure 5. Comparison of the Co 2*p* photoelectron spectra on the LSC_{113} single phase thin film (17) and on the LSC_{214} single phase thin film on STO substrates as a function of temperature at ultra-high vacuum (~10^{-9} mbar). Figure adapted from ref. (9).

In light of the observations above, we proposed that the electronic activation of LSC_{214} in the ML structure is caused by injection of electrons from LSC_{113} to LSC_{214} across their interface. It has been reported that the excess electrons in the lattice accompany the creation of oxygen vacancy defects on transition metal oxides decrease the electronegativity of the surface (21,22). Since it is easier for oxygen vacancy to form in LSC_{113}, the reduction in electronegativity (and the rising of the Fermi Level) is expected to be larger for LSC_{113} as compared to that for LSC_{214} at high temperatures. Such difference in the relative change in electronegativity would result in a band alignment that facilitates the electron injection from LSC_{113} to LSC_{214}. This could be accompanied by the Fermi level rising into the conduction band of LSC_{214}, leading to the apparent disappearance of the surface energy gap.

Impact on Oxygen Reduction Activity

LSC_{113} is a widely-studied mixed electronic and ionic conductor, which can be easily reduced and form electronic defect states that facilitate electron transfer to adsorbing oxygen species on its surface (17). The oxygen reduction on LSC_{113} is primarily limited

by the availability and mobility of surface oxygen vacancies (23). On the other hand, LSC_{214} is expected to exhibit very high oxygen incorporation and oxygen diffusion kinetics on the (100) plane, due to its capability to accommodate oxygen interstitials within the rock salt layers. At intermediate temperature (500-600 ^{o}C), the ORR process on LSC_{214} phase(24), similarly to other RP phase cathodes materials such as Nd_2NiO_4 (25) and $(La,Sr)_2MnO_4$ (26) was shown to be mainly limited by the electron transfer process. This behavior is related to the low electronic conductivity, large energy gap, and deficiency of electronic carriers in the conduction band on the surface of these materials. The strongly anisotropic oxygen incorporation kinetics on LSC_{214} (100) was predicted to be to 10^2 times faster in ORR kinetics compared to the (001) surface, by the theoretical work from our group (7). The (100) surface was exposed to ambient at the $LSC_{214/113}$ interface in the previous SIMS and electrochemical experiments. In this work we observed the electronic activation effect in LSC_{214} phase at high temperature through the contact with LSC_{113} phase.

Based on the facts above, we hypothesize that electronic activation of LSC_{214}, in concert with its anisotropically fast oxygen incorporation kinetics, is likely the key mechanism governing the fast oxygen reduction kinetics observed near $LSC_{113/214}$ interfaces. Firstly, excess electrons are generated accompanying the vacancy creation on/near the surface of LSC_{113} at high temperatures, as shown in Fig. 6. Those electrons were then injected from LSC_{113} into LSC_{214} (likely along with an exchange of oxygen vacancies and interstitials across the interface), which leads to the electronic activation of the LSC_{214} phase. The electronic activation and reduced electronegativity of the LSC_{214} phase (with an increased Fermi level) can facilitate charge transfer from LSC_{214} to the adsorbed oxygen.

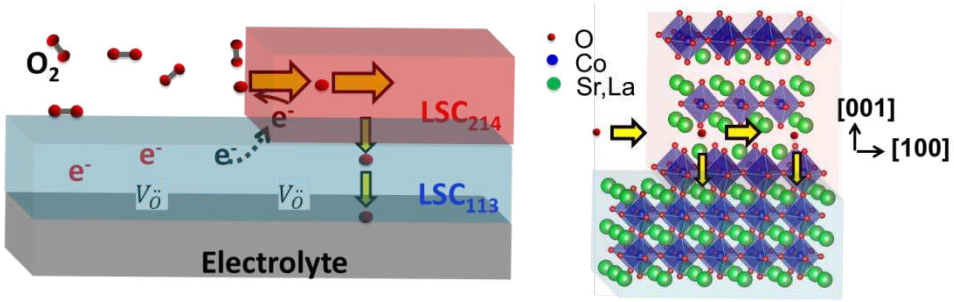

Figure 6. Mechanism that governs the enhancement of ORR activity at the interface of LSC_{113} and LSC_{214} layers. At high temperature, excess electrons from the reduced surface of LSC_{113} are injected across the interface into LSC_{214}, facilitating the charge transfer process at the LSC_{214} (100) surface. Figure adapted from ref. (9).

Our result points out that a wide-band-gap oxide can be electronically activated by charge injection due to the defect states of a neighboring reducible oxide phase. This new knowledge put forward a new concept of “electronically coupled composite cathodes” to further accelerate the fast oxygen incorporation path on the RP phase materials. We further test the validity of this model on the LSC_{113}/La_2NiO_4 (LSC_{113}/LNO_{214}) hetero-system, in which La_2NiO_4 is another oxide with highly anisotropic oxygen interstitial incorporation kinetics, and carries similar electronic characteristics (wide band gap) as LSC_{214}.

We fabricated LSC_{113}/LNO_{214} multilayer, LSC_{113} and LNO_{214} single phase films by PLD. With the same approach we defined above, we probed the electronic structure of LSC_{113} and LNO_{214} phase in both the ML structure and in single phase at high temperature. Fig. 7 shows the comparison of band gap value for LSC_{113} and LNO_{214} in ML structure and in single phase. We can see that the LSC_{113} surface electronic structure in the ML structure again behaves very similarly to its single-phase counterpart at high temperatures (17). Remarkably, the electronic structure of LNO_{214} in the ML differs significantly from its single phase by showing a reversible disappearance of the energy gap at and above 250 ^{o}C. At 300 ^{o}C, while LNO_{214} in ML has no band gap, LNO_{214} single phase film surface still presents about 1.3 eV band gap. This result indicates that a similar electronic activation effect exists for the LSC_{113}/LNO_{214} system. In our ongoing work, we are quantifying the ORR activity for LNO_{214} single phase, LSC_{113} single phase and LNO_{214} decorated LSC_{113} films with LSC_{113}/LNO_{214} interfaces on their surfaces. Our preliminary results indicate that LNO_{214} decorated LSC_{113} films could have better performance than the LSC_{113} and the LNO_{214} alone. Given the electronic activation of the LSC_{113}/LNO_{214} system, we believe that the "electronically coupled composite cathodes" concept can be expanded to other hetero-oxide systems, beyond the $LSC_{113/214}$. This opens a new way to synthesize high performance cathode structures.

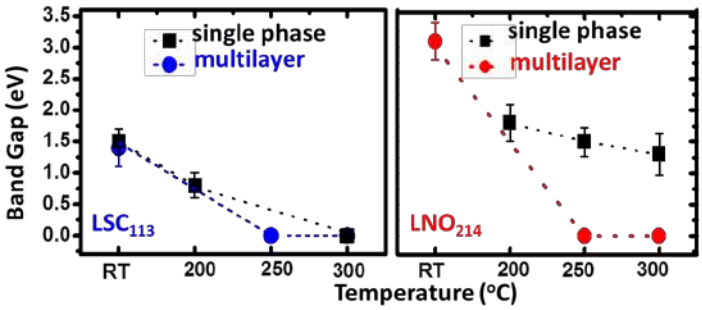

Figure 7. Energy gap values obtained on LSC_{113} and LNO_{214} when they are within the ML structure versus values obtained for the single phase thin film structures. The data on the single phase LSC_{113} films come from our previous report.(17)

Conclusion

In this study, we use a novel combination of *in-situ* scanning tunneling microscopy/spectroscopy and focused ion beam milling to probe the local electronic structure of $LSC_{113/214}$ model multilayer super lattice at high temperature and oxygen environment. Our results show that while the LSC_{113} in the ML structure behaves similar to its single-phase counterpart at high temperatures (200-300 ^{o}C), the LSC_{214} is electronically activated through an interface coupling with LSC_{113}. This is evidenced from the electronic structure of LSC_{214} that differs significantly from its single phase counterpart by exhibiting a large density of states near the Fermi level similar to that on LSC_{113}. Such electronic activation, concurrent with the anisotropic oxygen incorporation kinetics on the LSC_{214}, is expected to facilitate charge transfer to oxygen near the $LSC_{113/214}$ interface, explaining the vastly accelerated ORR kinetics. Our results put forward a new understanding of oxide hetero-interfaces at high temperatures and points towards electronically coupled oxide structures as novel cathodes. We further generalized and tested the validity of this model on the LSC_{113}/La_2NiO_4 hetero-system, in which

La_2NiO_4 remarkably shows the same electronic activation effect. Our results point out a novel route to obtain high performance cathode structures for intermediate temperature SOFCs.

Acknowledgments

Authors acknowledge the US-DOE - Basic Energy Sciences, Grant No. DE-SC0002633 for financial support. The FIB milling process and the X-ray diffraction and Auger electron spectroscopy measurements were performed at the Center of Materials Science and Engineering, an NSF MRSEC facility at MIT.

References

1. E. D. Wachsman, C. A. Marlowe and K. T. Lee. *Energy & Environmental Science* **5**, 5498 (2012).
2. A. J. Jacobson. *Chemistry of Materials* **22**, 660 (2010).
3. M. Sase, K. Yashiro, K. Sato, J. Mizusaki, T. Kawada, N. Sakai, K. Yamaji, T. Horita and H. Yokokawa. *Solid State Ionics* **178**, 1843 (2008).
4. M. Sase, F. Hermes, K. Yashiro, K. Sato, J. Mizusaki, T. Kawada, N. Sakai and H. Yokokawa. *Journal of the Electrochemical Society* **155**, B793 (2008).
5. K. Yashiro, T. Nakamura, M. Sase, F. Hermes, K. Sato, T. Kawada and J. Mizusaki. *Electrochemical and Solid State Letters* **12**, B135 (2009).
6. E. J. Crumlin, E. Mutoro, S. J. Ahn, G. J. la O, D. N. Leonard, A. Borisevich, M. D. Biegalski, H. M. Christen and Y. Shao-Horn. *Journal of Physical Chemistry Letters* **1**, 3149 (2010).
7. J. W. Han and B. Yildiz. *Energy & Environmental Science* **5**, 8598 (2012).
8. M. J. Gadre, Y. L. Lee and D. Morgan. *Physical Chemistry Chemical Physics* **14**, 2606 (2012).
9. Y. Chen, Z. Cai, Y. Kuru, W. Ma, H. L. Tuller and B. Yildiz. *Advanced Energy Materials*, DOI: 10.1002/aenm.201300025 (2013).
10. J. Suntivich, H. A. Gasteiger, N. Yabuuchi, H. Nakanishi, J. B. Goodenough and Y. Shao-Horn. *Nat Chem* **3**, 546 (2011).
11. W. Jung and H. L. Tuller. *Advanced Energy Materials* **1**, 1184 (2011).
12. Y.-L. Lee, J. Kleis, J. Rossmeisl, Y. Shao-Horn and D. Morgan. *Energy & Environmental Science* **4**, 3966 (2011).
13. A. Kumar, F. Ciucci, A. N. Morozovska, S. V. Kalinin and S. Jesse. *Nat Chem* **3**, 707 (2011).
14. M. Basletic, J. L. Maurice, C. Carretero, G. Herranz, O. Copie, M. Bibes, E. Jacquet, K. Bouzehouane, S. Fusil and A. Barthelemy. *Nature Materials* **7**, 621 (2008).
15. T. Y. Chien, J. A. Liu, J. Chakhalian, N. P. Guisinger and J. W. Freeland. *Physical Review B* **82**, 041101 (2010).
16. Y. Kuru, H. Jalili, Z. H. Cai, B. Yildiz and H. L. Tuller. *Advanced Materials* **23**, 4543 (2011).
17. Z. H. Cai, Y. Kuru, J. W. Han, Y. Chen and B. Yildiz. *Journal of the American Chemical Society* **133**, 17696 (2011).

18. K. Katsiev, B. Yildiz, K. Balasubramaniam and P. A. Salvador. *Applied Physics Letters* **95**, 092106 (2009).
19. Y. Chen, W. C. Jung, Z. Cai, J. J. Kim, H. Tuller and B. Yildiz. *Energy & Environmental Science* **5**, 7979 (2012).
20. V. V. Vashook, H. Ullmann, O. P. Olshevskaya, V. P. Kulik, V. E. Lukashevich and L. V. Kokhanovskij. *Solid State Ionics* **138**, 99 (2000).
21. N. A. Deskins, R. Rousseau and M. Dupuis. *Journal of Physical Chemistry C* **114**, 5891 (2010).
22. M. T. Greiner, M. G. Helander, W. M. Tang, Z. B. Wang, J. Qiu and Z. H. Lu. *Nature Materials* **11**, 76 (2012).
23. Y. A. Mastrikov, R. Merkle, E. Heifets, E. A. Kotomin and J. Maier. *Journal of Physical Chemistry C* **114**, 3017 (2010).
24. B. Peng, G. Chen, T. Wang, J. Zhou, J. J. Guo, Y. H. Cheng and K. Wu. *Journal of Power Sources* **201**, 174 (2012).
25. A. Yamada, Y. Suzuki, K. Saka, M. Uehara, D. Mori, R. Kanno, T. Kiguchi, F. Mauvy and J. C. Grenier. *Advanced Materials* **20**, 4124 (2008).
26. L. P. Sun, Q. Li, L. H. Huo, H. Zhao, G. Y. Zhang, N. Lin, J. P. Viricelle and C. Pijolat. *Journal of Power Sources* **196**, 5835 (2011).